



Diagnostic evaluation of numerical air quality models with specialized ambient observations: testing the Community Multiscale Air Quality modeling system (CMAQ) at selected SOS 95 ground sites

J.R. Arnold^{a,*}, R.L. Dennis^{a,1}, G.S. Tonnesen^b

^a *Atmospheric Sciences Modeling Division, National Oceanic and Atmospheric Administration, Air Resources Laboratory, Research Triangle Park, NC 27711, USA*

^b *Center for Environmental Research and Technology, University of California, Riverside, CA 92521, USA*

Received 3 August 2002; accepted 13 November 2002

Abstract

Three probes for diagnosing photochemical dynamics are presented and applied to specialized ambient surface-level observations and to a numerical photochemical model to better understand rates of production and other process information in the atmosphere and in the model. However, care must be taken to ensure that rate and process information is not confounded by inappropriate averaging over these diurnally changing photochemical dynamics. One probe, the $[O_3]$ response surface probe $[O_3]/[NO_x]$, is used here as a chemical filter to select NO_x -limited hours in the observations and the simulations. Other probes used here are the fraction NO_z/NO_y , a measure of chemical aging, and a measure of the production efficiency of O_3 per NO_x converted, $[O_3]$ to $[NO_z]$. The key ambient measurements for all three probes are accurate $[NO_2]$ and a reliable estimate of total NO_y . Good agreement is shown between models and observations in cases where local photochemical production dominates and where model emissions inputs are thought to be mostly complete. We interpret this agreement to mean that the photochemical processing in CMAQ is substantially similar to that in the atmosphere. More importantly, we see that the three probes provide consistent information about photochemical processing, especially when used together.

© 2003 Published by Elsevier Science Ltd.

Keywords: Photochemical modeling; Model evaluation; Ozone sensitivity indicators; Carbon Bond IV; Southern Oxidants Study

1. Introduction

Urban and regional air quality is determined by a complex system of coupled chemical and physical processes including emissions of pollutants and pollutant precursors, complex chemical reactions, physical transport and diffusion, and wet and dry deposition. This system has long been known to be nonlinear in

production of ozone ($P(O_3)$) and other secondary pollutants (Dodge, 1977), to extend over multiple spatial and temporal scales, and to involve complicated cross-media environmental issues such as acidic or nutrient deposition to ecosystems and visibility degradation.

Ozone remains a pollutant of special concern both because of its widespread effects on ecological and human health (National Research Council, 1991) and its key position in the processes and cycles affecting the formation and fate of other pollutants (Seinfeld and Pandis, 1998). Without correctly understanding those coupled nonlinear processes, there is greater risk for error when using numerical photochemical air quality

*Corresponding author.

¹ On assignment to the National Exposure Research Laboratory, US Environmental Protection Agency/Office of Research and Development, Research Triangle Park, NC 27711, USA.

model (AQM) estimates for developing and evaluating emissions control strategies. Because large economic and social costs attach to air pollutant control—the estimated annual cost of compliance with urban and regional O₃ regulations alone is in excess of US \$1 billion (US EPA, 1997)—we wish to reduce the risk of error by using scientifically advanced AQMs to provide a realistic simulation of future conditions and an accurate appraisal of the type and amount of emissions control necessary to meet mandated air quality goals.

The oxidized nitrogen species collectively labeled NO_Y (NO_Y = NO_XNO + NO₂) + nitrate radical + nitric acid + nitrous acid + peroxyacetyl nitrate + other organic nitrates + other lesser contributing oxidized nitrogen compounds) control the production and fate of O₃ and aerosols by sustaining or suppressing hydroxyl radical (OH) cycling. Characterizing the interrelated NO_Y and OH dynamics for O₃ formation and fate in the polluted troposphere depends on new techniques using combinations of several NO_Y species for diagnostically probing the complex atmospheric dynamics in typical urban and regional airsheds. Dennis et al. (2000) provides more detail on measurement requirements for diagnostic model evaluation. Here we use the example of diagnosing P(O₃) both in ambient observations and in model simulations with the US EPA Community Multiscale Air Quality modeling system (CMAQ) to illustrate the utility of high-quality ambient measurements of selected NO_Y species, most especially NO₂.

2. Diagnostic evaluation of numerical photochemical process models

2.1. Ozone production processes and the ozone response surface

Ozone in a model grid cell or from an observation results from complex interactions of multiple atmospheric processes acting over different spatial and temporal scales, processes including pollutant emissions, horizontal and vertical advection and diffusion, chemical production and loss, and deposition losses. The physical and chemical dynamics of these interactions are represented in AQMs using a set of coupled nonlinear partial differential equations to describe mathematically the mass conservation equation for each chemical species (Russell and Dennis, 2000)

$$\frac{\partial C_i}{\partial t} = -\nabla(\bar{U}C_i) + \nabla(K_c \nabla C_i) + P_i - L_i + E_i - R_i + \left. \frac{\partial C_i}{\partial t} \right|_{\text{clouds}} \quad \text{for } i = 1, \dots, N, \quad (1)$$

where N is the number of chemical species represented in the AQM, C_i is the concentration of species i , \bar{U} is the wind vector, K_c is the turbulent diffusion coefficient, E_i

is the emissions source term for species i , R_i is the removal term for species i via various processes (for example dry and wet deposition), P_i is the chemical production term for species i , L_i is the loss rate of species i via gas-phase chemical reactions, and $(\partial C_i / \partial t)_{\text{clouds}}$ is the production and/or loss of species i by cloud or aqueous-phase chemical processes.

Fig. 1 shows, using the example of CH₄, a reaction pathway schematic for the interrelated cycling of OH and NO_X in the production of O₃. Because the chemistry of O₃ formation is highly nonlinear, changing either NO_X or volatile organic compound (VOC) emissions can alter the system's P(O₃), but changes in P(O₃) are not monotonic with these precursor changes.

Fig. 2 shows a 3D response surface of the maximum O₃ mixing ratio ([O₃]) to various levels of NO_X and VOC from a simulation for Atlanta, GA, made using a photochemical trajectory model. (Description of the model setup is found in Tonnesen and Dennis, 2000a.) Isoleth lines on the response surface are derived by fitting contours to the peak predicted [O₃] in multiple model simulations using different initial NO_X and VOC emissions. Note that many different combinations of NO_X and VOC emissions can produce the same [O₃], showing that solutions to Eq. (1) are nonunique. The heavy dotted line drawn across the ridges of the surface contour lines in Fig. 2 is the ridgeline of maximum [O₃] and divides the response surface into two regions where P(O₃) is limited in different ways. To the right of the response surface ridgeline, P(O₃) is limited by NO_X availability, so reductions in NO_X decrease P(O₃) and VOC reductions have little influence. To the left of the ridgeline, radical availability and NO_X inhibition limit P(O₃), so reductions in NO_X can increase P(O₃) while VOC reductions reduce P(O₃). Although the shape of an O₃ response surface is determined by the P(O₃) nonlinearities changing with changing NO_X and VOC levels, the photochemical system is also responsive to changes other than in NO_X and VOC emissions levels, to different meteorology or to different chemical mechanism representations, for example.

As Fig. 1 shows, P(O₃) dynamics are governed by the initiation, propagation, and termination of a small number of important radical species that preferentially attack either VOCs or NO_X as concentrations of all species in the pollutant mix change through time and space. P(O₃) begins with the initiation of new radicals primarily from O₃ in rural or other NO_X-limited areas, but also from formaldehyde (HCHO), and nitrous acid (HONO). Radicals are propagated through the system as RO₂ and HO₂ are formed following OH attack on VOCs and setting up the OH recreation cycle. To help describe this cycle, a few terms will be defined here. The OH propagation efficiency (Pr_{OH}) is defined as the average fraction of OH recreated for the cycle of OH reactions. The OH chain length is defined as the average

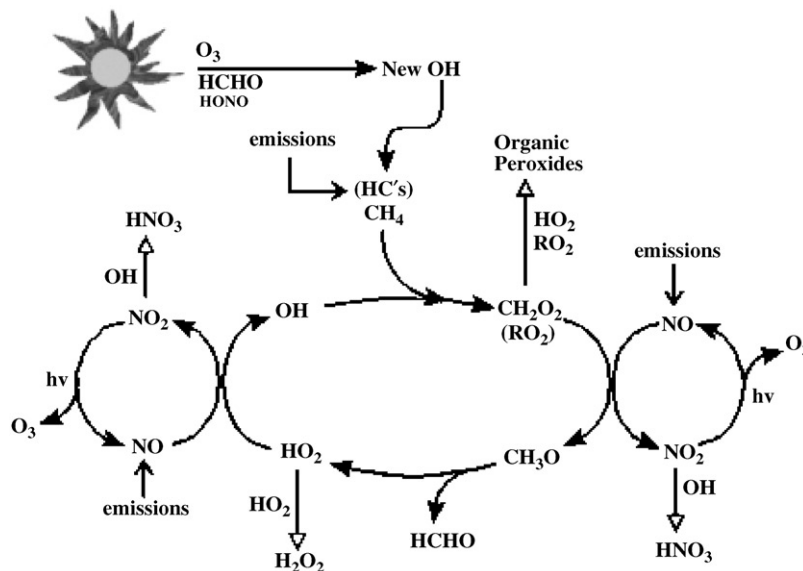


Fig. 1. Schematic of the interrelated cycles of OH initiation, propagation, and termination, and NO_x transformation using the example of CH₄.

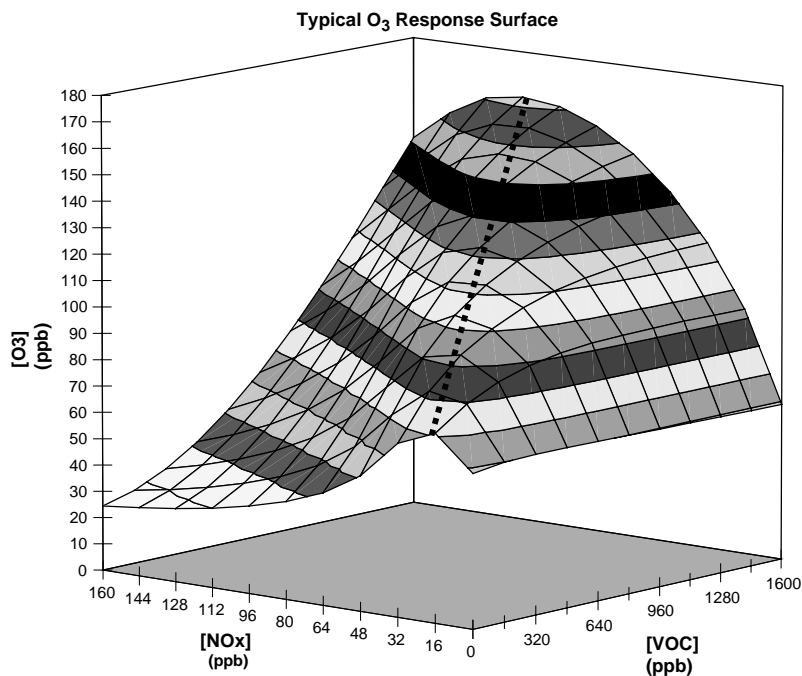


Fig. 2. Nonlinear [O₃] response surface for changes in initial NO_x and VOCs indicating regions of radical and NO_x sensitivities and the ridgeline of maximum [O₃] (heavy dotted line) between them.

number of times a new radical cycles through the system until being removed in a termination reaction, calculated as

$$\begin{aligned} \text{OH chain length} &= 1 + Pr_{\text{OH}} + Pr_{\text{OH}}^2 + Pr_{\text{OH}}^3 + \dots \\ &= 1/(1 - Pr_{\text{OH}}). \end{aligned} \quad (2)$$

Fig. 1 also shows the companion NO_x cycle to the OH one with a similarly defined chain length in which NO is recreated and cycled until terminated. Like P(O₃), OH and NO_x chain length vary in space and time as the relative availabilities of VOCs and NO_x change. The number of molecules processed through these reactions

can be large compared to an instantaneous mixing ratio, but OH and NO_x chain lengths in the troposphere are generally less than 10.

The [O₃] ridgeline on the response surface in Fig. 2 can now be explained in terms of these VOC–OH–NO_x dynamics. The rate of P(O₃) is approximately proportional to the rate of OH attack on VOCs and is maximized for conditions that maximize the total rate of OH production (P(OH)), which is the product of OH initiation and OH chain length as in Eqs. (3) and (4)

$$P(O_3) \approx k(OH + VOC), \quad (3)$$

$$P(OH) = OH_{\text{initiated}} \times 1/(1 - Pr_{OH}). \quad (4)$$

Because of the inverse dependence of P(OH) on (1–Pr_{OH}), P(O₃) will be maximized for conditions that maximize Pr_{OH}, thereby creating the [O₃] ridgeline in Fig. 2.

Systems with a low VOC/NO_x ratio are found to the left of that ridgeline where P(O₃) is limited by the availability of radicals. Under conditions of high [NO_x] in this radical-limited region, NO₂ reacts with OH and terminates to HNO₃, removing both OH and NO₂ in one step, which limits P(O₃) by reducing the production of OH. Furthermore, excess NO in this region titrates O₃ back to NO₂, reducing O₃ photolysis as a source of new OH. Here the efficiency of P(O₃) per NO_x terminated is low and P(O₃) is more responsive to reductions in VOCs than in NO_x. In fact, as Fig. 2 shows, reducing NO_x emissions without concomitant VOC reductions for photochemical systems in this region can cause increases in final [O₃].

Conditions to the right of the ridgeline with high VOC/NO_x ratios are quite different. There, [NO] is relatively low, allowing HO₂ and RO₂ radicals to self-terminate. This reduces the number of times OH can be propagated and so lowers the efficiency of P(O₃) per radical. Termination of NO₂ by OH to HNO₃ (as above) is also reduced because less NO₂ is available for termination and because a larger radical pool means radical–radical termination pathways are preferred. Hence in these cases, although the efficiency of P(O₃) per NO_x terminated is high, less NO_x is available for reacting, resulting in lower P(O₃) and a lower final [O₃]. In this NO_x-limited region, therefore, P(O₃) is more responsive to reductions in NO_x than VOCs. But even though VOC emission reductions are less effective in reducing [O₃] here, reductions in either precursor are expected to decrease [O₃].

2.2. Specific diagnostic tests of photochemical dynamics in urban and regional airsheds

We previously described (Arnold et al., 1998) a model evaluation methodology that distinguishes several types of AQM testing. Two components of that methodology

are operational testing to judge the performance and overall behavior of a model over specific attributes, and diagnostic testing to help reveal potential compensating error in model inputs or processing. Diagnostic testing is in situ testing of model components using data that emphasize atmospheric processes, often with mass balance techniques, special species ratios, and process rate and reaction rate information not typically stored by the model for output. We have developed some of these probes through process-oriented studies using theoretical assumptions, model-derived explanations, and results from instrumented models ranging from 1D box models to the full 3D photochemical modeling system (see Tonnesen and Dennis, 2000a, b). Additional information on instrumenting AQMs for diagnostic analysis with model process and reaction rate information is found in Dennis et al. (2002); information pertaining to the specific implementation of these techniques in CMAQ is found in Gipson (1999).

Table 1 shows a listing of diagnostic elements that can be used to probe the photochemical dynamics of P(O₃).

The first category of individual dynamics components includes initiation of new radicals from O₃, HCHO, and HONO, and termination of radical cycling either as peroxy radicals self-combine and/or OH and NO₂ are converted to the relatively stable oxidized nitrogen products NO_z, (NO_z = NO_y–NO_x). The probe of air mass aging, [NO_z]/[NO_y], which we describe here is drawn from this category.

The second category of photochemical process groupings includes propagation of radicals through the system as HO₂ radicals are formed and convert NO to NO₂,

Table 1
Diagnostic elements of photochemical dynamics

Individual component aspects	Radical initiation Radical termination Competition between termination pathways Air mass aging
Process aspects	OH production Radical propagation Radical propagation efficiency, Pr(OH) OH chain length NO _x chain length P(O ₃) efficiency per NO _x termination
Response surface aspects	System state relative to ridgeline Location of ridgeline in response space Slope of radical-limited response surface Slope of NO _x -limited response surface

and the related concepts of Pr_{OH} and chain length as defined above. The cycle of OH radicals through attack on VOCs with production of HO_2 is closely bound to the conversion of NO to NO_2 such that excess availability of one species, NO, ensures OH propagation and excess availability of the other, NO_2 , leads to OH termination. From this category, we report results here from testing a probe of O_3 production efficiency, $[O_3]$ vs. $[NO_x]$.

The third category includes elements of the integrated response of a photochemical system such as that represented on the $[O_3]$ response surface shown in Fig. 2. Tests from this category probe a model's ability to track the photochemical system's change of state and generally involve use of species and ratios of species concentrations thought to correlate consistently with VOC- and NO_x -sensitive $P(O_3)$. Tests that probe this systematic change have been referred to as "indicators" of control strategy sensitivity as described in Kleinman (1994), Milford et al. (1994), Sillman (1995), and Sillman et al. (1997). These measures of the sensitivity of O_3 to NO_x and VOC changes are characteristics of specific photochemical systems in that each system may have particular combinations of NO_x and VOCs that determine its position on the $[O_3]$ response surface in one region or the other. However, we have observed in the model that individual systems exhibit a strong diurnal behavior, too, moving from strongly radical-limited in the morning to the transition state near the $[O_3]$ ridgeline and on into the NO_x -limited region of the response surface later in the day. Tracking this air mass history with cumulative diagnostics is important for understanding the model's behavior for its intended use in control strategy development and assessment since, as shown above, the position of a system in one or the other regions of the response surface determines whether VOC or NO_x controls are to be preferred. In this paper, we discuss one proposed indicator ratio, $[O_3]/[NO_x]$.

3. Observations data set and model configurations

3.1. SOS 95 surface site observations

The 1995 Southern Oxidant Study Nashville/Middle Tennessee Ozone Study (SOS 95) included comprehensive air quality field experiments on multiple aircraft platforms and at several highly instrumented surface sites in and around the city of Nashville (see Meagher et al. (1998) for the study overview). The "level 2" and "level 3" sites (Olszyna et al., 1998) were specially instrumented for continuous observations of a number of chemical species and meteorological state variables and we have examined many of these data in our wider testing and evaluation of CMAQ. The diagnostic testing presented here has focused on continuous O_3 , NO,

accurate NO_2 (at these sites by photolytic reduction), and total NO_y measurements at three of the level 2 and level 3 sites: Dickson, ~60 km west of Nashville and designated an urban-suburban chemistry site by SOS 95 study planners, but one strongly influenced by large point sources including the Cumberland and Johnsonville power plants; Giles, ~150 km south of Nashville and designated a regional chemistry site, though one having previously unexpected local NO_x sources as well; and Youth, ~25 km southeast of Nashville and designated an urban-suburban chemistry site. Fig. 3 shows a map of chemistry sites and local sources in the SOS 95 domain. Fuller description of the configuration of these sites and experimental details of the data are given in Olszyna et al. (1998).

3.2. CMAQ configurations and modeled domains

CMAQ is the comprehensive modeling system developed by the US Environmental Protection Agency's Office of Research and Development. It is a comprehensive urban-to-regional scale Eulerian photochemical air quality process model designed for assessments of multiple pollutants including O_3 and other oxidants, aerosols, and acid/nutrient deposition to ecosystems. CMAQ is an open-source, community-supported model; more detailed descriptions of CMAQ including its theoretical formulations, chemical and physical process parameterizations, numerical algorithms, and complete mechanism listings are found in Byun and Ching (1999). Additional and updated documentation, links to other model evaluation results, and the modeling system itself are available at <http://www.epa.gov/asmdnerl/models3>.

In the model simulations we report here, the NCAR/Penn State fifth-generation mesoscale model MM5 (Grell et al., 1994) was used as the meteorological driver. MM5 v2.10 was configured in nonhydrostatic mode, having 30 sigma layers with the surface layer nominally 38 m, with one-way nested grids, and with analysis nudging of winds but not temperature or moisture within the PBL in the 108, 36, and 12 km grids, but no nudging of any kind in the 4 km grid.

For emissions processing and projection a combination of two models, the Models-3 Emissions Processing and Projection System (Benjey et al., 1999) and MCNC's Sparse Matrix Operator Kernel Emissions (SMOKE) processors (<http://www.emc.mcnc.org/products/smoke/>), were used. Typical summer day emissions were generated with large elevated point source estimates replaced by continuous emissions monitoring observations where available.

The CMAQ chemical transport model (CCTM) was run with 21 vertical layers compressed from the MM5 30 layers but keeping 11 layers in the lowest 1000 m. Horizontal grids were one-way nested at 36, 12, and 4 km as shown in Fig. 4, although results presented here

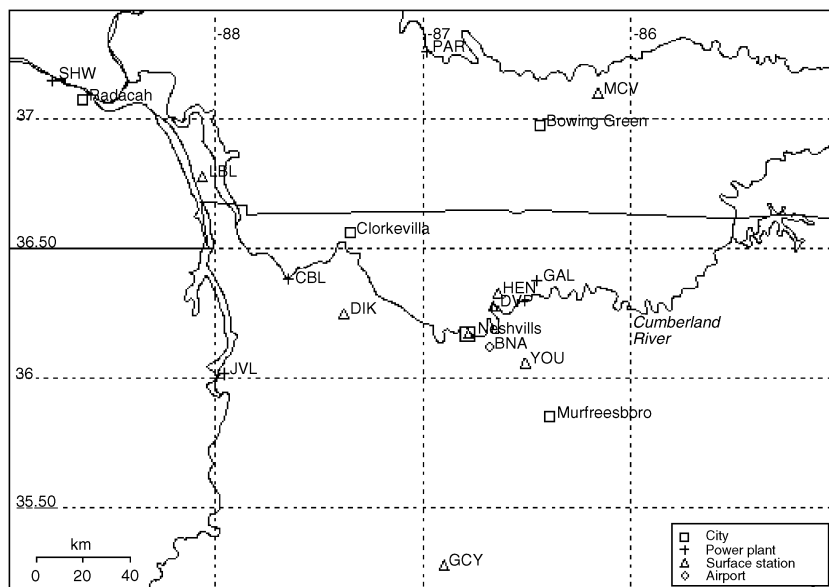


Fig. 3. Map of the SOS 95 surface sites Dickson (DIK), Giles (GCY), and Youth (YOU), urban areas, and nearby power plants Cumberland (CBL), Johnsonville (JVL), and Gallatin (GAL). From Senff et al. (1998).

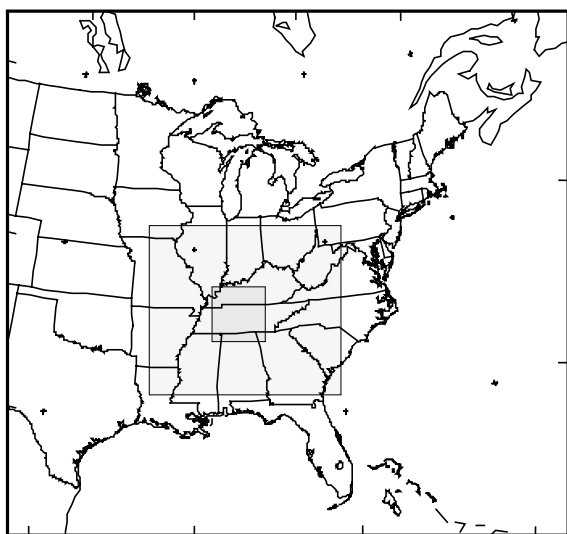


Fig. 4. One-way nested CMAQ model domains for SOS 95: 36 km outer, 12 km middle, 4 km inner.

are from only the two finer scale grids in the interest of clarity.

Two chemical mechanisms were run, Carbon Bond IV (CB4) (Gery et al., 1989) and the Regional Acid Deposition Model chemistry, version 2 (RADM2) (Stockwell et al., 1990). The CB4 version used for these runs includes 64 species and operators in 97 gas-phase and aerosol reactions with a one-product reaction set for

isoprene. RADM2 includes 93 species and operators in 200 gas-phase and aerosol reactions with a 4-product isoprene implementation. Both isoprene reaction sets were implemented following the work of Carter (1996). Models with both mechanism versions were run with the SMVGEAR solver (Jacobson and Turco, 1994). The CCTM includes aerosol emissions, RADM-type dry deposition with the resistance-in-series method, and RADM-type aqueous cloud processes.

We report here from a CMAQ modeling series for 5–18 July 1995, a 2-week period that includes both the highest recorded $[O_3]$ of the 6-week SOS 95 field intensive as noted by Valente et al. (1998) and several days with low $[O_3]$ maxima following frontal passage clean out of the atmosphere. This evaluation period was intentionally designed to cover this range of different chemical regimes to ensure against any potential bias from only high or low O_3 event days. The first model evaluation day, 5 July, was preceded by four days of model spin up to ensure against undue influence from model initial conditions.

4. Results

4.1. Response surface probe: $[O_3]/[NO_x]$

We previously evaluated (Tonnesen and Dennis, 2000a,b) our response surface indicator $[O_3]/[NO_x]$ along with several other potential indicator ratios suggested by other researchers (chiefly Sillman, 1995;

Sillman et al., 1997) in a series of model simulations to characterize their degree of precision across space and time. That work demonstrated that none of the proposed measures indicates the relative sensitivity of the photochemical system to emissions changes with high precision in all cases. However, $[O_3]/[NO_x]$ performed no worse than the other indicators and has the advantage that it can be tested more widely than some other suggested measures requiring more difficult ambient observations of H_2O_2 or HNO_3 , for example. Tonnesen and Dennis (2000b) also showed that $[O_3]/[NO_x]$ appeared to indicate reliably a photochemical system's position on the $[O_3]$ response surface relative to the ridgeline. Values of the ratio <15 indicate the strongly radical-limited, NO_x -inhibited and hence VOC-sensitive conditions often prevalent at the surface during peak morning commutes or in fresh power plant plumes. Values >46 indicate a position across the $[O_3]$ ridgeline, well into the NO_x -limited and hence NO_x -sensitive region.

One useful way to characterize the movement of photochemical systems from radical-limited to NO_x -limited regions of the response surface is to bin the total hours spent in each extreme region and nearer to the $[O_3]$ ridgeline according to the indicator value. For this analysis bin thresholds were first estimated from our previous work with the indicator which showed that a general range of values holds over most conditions (Tonnesen and Dennis, 2000b), and then were refined using indicator values at the three sites from observations only and not from the model. For example, we established the general range of indicator values for the ridgeline by determining the point at which $P(O_3)$ appeared to have increased such that NO_x titration was no longer dominant and $[O_3]$ was increasing. Figs. 5(a–c) show histograms for each of the three sites binned to show the strongest radical-limited hours (values <14), the strongest NO_x -limited hours (values >46), and two bins near the response surface ridgeline between the extremes around the indicator value 15. Values in the histograms are given for the observations at each site and for the model with 12 and 4 km grid spacings and with CB4 and RADM2 chemistries, and were calculated for all hours in the model for which an observation was reported at the site. Total hours at each site vary due to variation in the operation time of each site's NO_2 instrument.

For the most part, CMAQ correctly reproduces the distributions of the observed indicator values across the different conditions represented at the three sites. Discrepancies in the >46 range at the near-urban Youth site are smaller with the 4 km model than the 12 km, and this result is consistent with comparisons we have made (not shown here) demonstrating better operational performance by the 4 km models (Arnold and Dennis, 2001). Some discrepancies at the rural

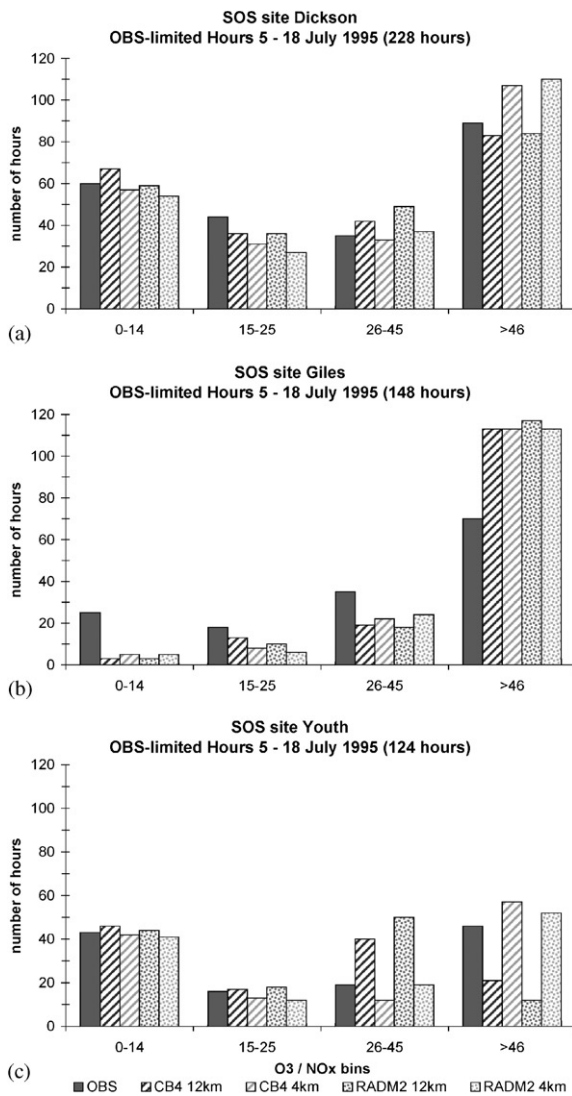


Fig. 5. (a)–(c) Response surface indicator distributions for observations and models at (a) Dickson, (b) Giles, and (c) Youth.

Dickson site appear due to excessive total NO_y (and hence NO_x) erroneously spread instantaneously into the grid domain from Cumberland power plant emissions plumes. Power plant plumes in the atmosphere retain more physical and chemical coherence than is present in the artificial model mixing that disperses instantly into the 12 or 4 km grid cells. This difference between the atmosphere and the grid model mixing may also explain why the 12 km model appears to be marginally better at Dickson than the 4 km since the 4 km would tend to concentrate still further the instantly dispersed plume NO_y in its smaller cell volume. Preliminary results (not shown here) from other CMAQ runs using the

additional embedded plume-in-grid model (PinG) (Gillani and Godowitch, 1999) demonstrate improvement on this test when instant plume dispersal is eliminated, and thus support this hypothesis. The large discrepancies across all indicator ranges at Giles appear due to a very local NO_x source not accounted for in CMAQ input emissions, a source which has also been noted by some of the SOS 95 surface site researchers in analysis of the Giles observations (Olszyna, 2002). Note that choice of the chemical mechanism, CB4 or RADM2, appears to make no significant difference to the indicator distributions at any of the sites at either grid spacing.

Figs. 6(a–c) show a view of model fits to observations using diurnal time to correlate temporally all observed hours every day at each site. Since the $[\text{O}_3]/[\text{NO}_x]$ response surface probe revealed no significant difference between the chemical mechanisms, only CB4 model results are shown. CMAQ reproduces both the temporal correlation and the amplitude of the majority of observed values at these sites. The diurnal time view in Fig. 6a shows clearly the effects of fresh NO_x plumes touching down at Dickson at nearly any hour. These NO_x intrusions create low response surface indicator ratios at midday and modify the standard diurnal curve of a photochemical system transitioning from the radical-limited region overnight, across the ridgeline as the photochemical day begins, and into the NO_x -limited region in the mid-afternoon. The consistent overprediction of the response surface indicator ratio by all models at Giles (Figs. 5b and 6b), perhaps due to an unreported local NO_x source as mentioned above, shifts the simulated distribution substantially into the NO_x -limited region much earlier and much further than the observations.

4.2. Individual components probe: $[\text{NO}_z]/[\text{NO}_y]$

The age of an air mass can usefully be represented as the fraction of NO_y converted to NO_z . Values of $[\text{NO}_z]/[\text{NO}_y] < 0.6$ indicate a fresher NO_x plume with an increased potential for O_3 production or loss, conditional on radical availability in the system; that is, on the system's position on the response surface. Higher values of the ratio indicate an aged air mass with less potential for change in O_3 .

Figs. 7(a–c) show diurnal time plots of the $[\text{NO}_z]/[\text{NO}_y]$ fraction for Dickson, Giles, and Youth, respectively. As with the response surface probe, results shown here are for CB4 chemistry only since little difference could be attributed to chemical mechanism. At Youth, CMAQ appears to be aging NO_x appropriately, reproducing the diurnal pattern quite well. At Dickson, more hours with fresher NO_x appear in the observations than in the model predictions but CMAQ does predict hours with fresh plumes arriving at Dickson as the $[\text{O}_3]/[\text{NO}_x]$

indicator had suggested. The largest discrepancies occur at Giles where the presence of fresh NO_x in the observations but not included in model emissions inputs is easily seen. The information given by the aging indicator, then, is fully consistent with that given by the response surface indicator for Giles, with the aging probe showing even more clearly the effect of fresh NO_x on the processing dynamics. Finally, the higher model ratios relative to the observations at Dickson suggest that where fresh plumes are present, the model may be processing more NO_x to NO_z than the observations. This difference is not notable at Youth where the model results are nearer to the observations ranges, and is not interpretable at Giles where the NO_x emissions error dominates.

An example where two diagnostic probes are used in concert is shown in Figs. 8(a–b) for Dickson and Youth, respectively; analogous plots for the emissions-affected Giles sites are not shown here for brevity. The scatterplots in Fig. 8 show how the response surface indicator value can be used as a chemical filter to select only those hours where the photochemical system is fully NO_x -limited using the $[\text{O}_3]/[\text{NO}_x]$ bin > 46 . CMAQ is aging the NO_x further than the atmosphere at Dickson but is closer to the observations at Youth. The weight of the distribution in both sets of plots, however, shows that at Youth at least, where photochemistry dominates, CMAQ is accumulating O_3 and aging NO_x generally in accord with the observations.

4.3. Process diagnostic probe: $[\text{O}_3]$ to $[\text{NO}_z]$

The slope of the line produced by plotting $[\text{O}_3]$ against $[\text{NO}_z]$ is a measure of the photochemical processing of NO_x referred to as the O_3 production efficiency, or the number of O_3 molecules produced for each NO_x processed to NO_z . (see Parish et al., 1993; Trainer et al., 1993; Kleinman et al., 1996a,b). The relation indicates both a cumulative $\text{P}(\text{O}_3)$ rate and the average NO_x chain length over an air mass history which often has been presented with observations or model results for all hours either observed or in the simulation. However, using all hours complicates interpretation of the test by mixing together rates from very different parts of the diurnal $\text{P}(\text{O}_3)$ cycle. To sharpen interpretation of this process diagnostic test, we select hours in the observations and the model filtered by the ridgeline indicator for the $[\text{O}_3]/[\text{NO}_x]$ range > 46 which ensures that the system is well out of the radical-sensitive region of the response surface. Chemical filtering using $[\text{O}_3]/[\text{NO}_x]$ is a more accurate means of segregating hours in the NO_x -limited domain than taking a subset of hours from daily afternoon periods as is sometimes done with $\text{P}(\text{O}_3)$ estimates (Olszyna et al., 1998, for example) and allows for analysis of different parts of the diurnal $\text{P}(\text{O}_3)$ dynamics.

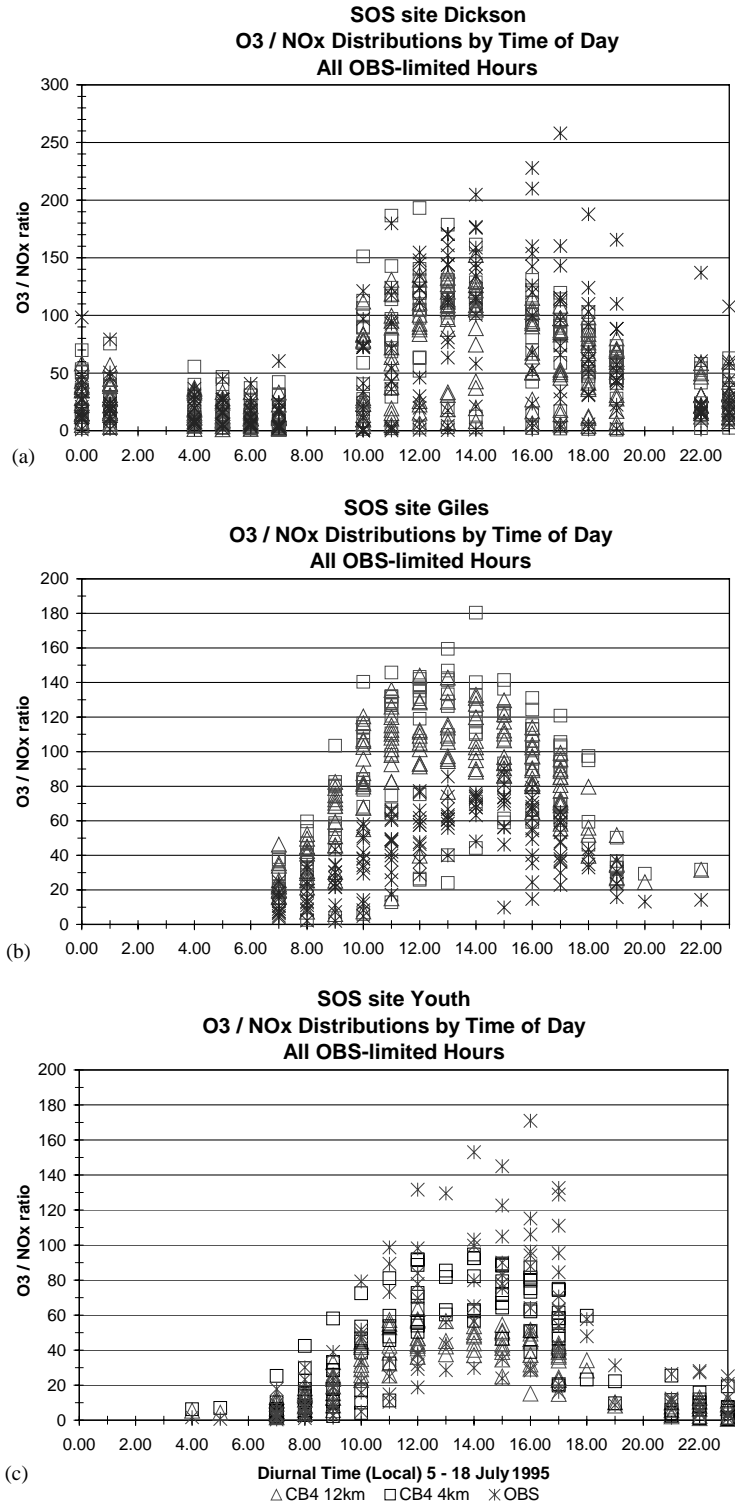


Fig. 6. (a)–(c) Response surface indicator distribution, CB4 chemistry only, by time of day for all days at (a) Dickson, (b) Giles, and (c) Youth.

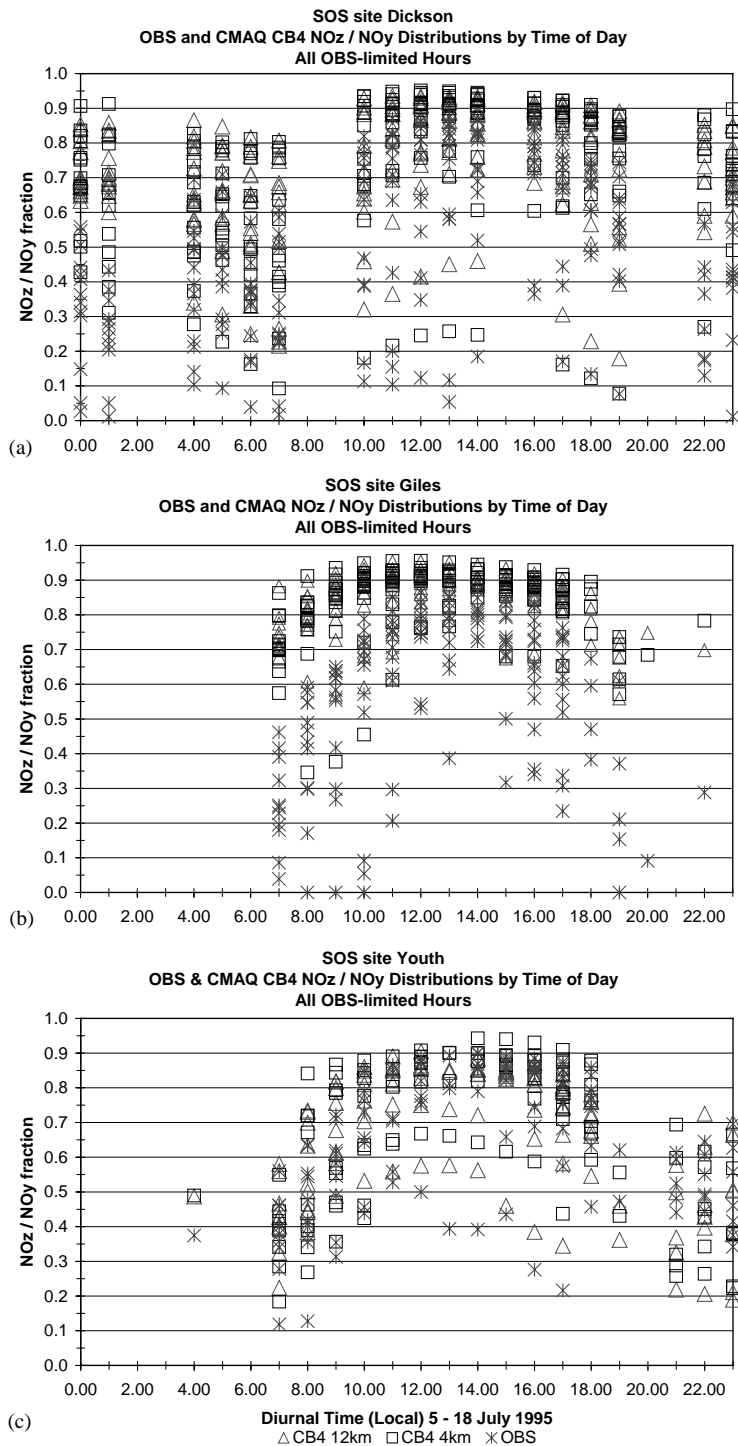


Fig. 7. (a)–(c) Photochemical age fraction for all days each hour, CB4 chemistry only, at (a) Dickson, (b) Giles, and (c) Youth.

Figs. 10(a) and (b) show scatterplots of O₃ to NO_Z for the Dickson and Youth sites for all hours for which there were observations and for which the ridgeline

indicator was > 46. As above, only model versions with CB4 chemistry are presented and no plots for Giles are shown for brevity. In general, CMAQ reproduces the

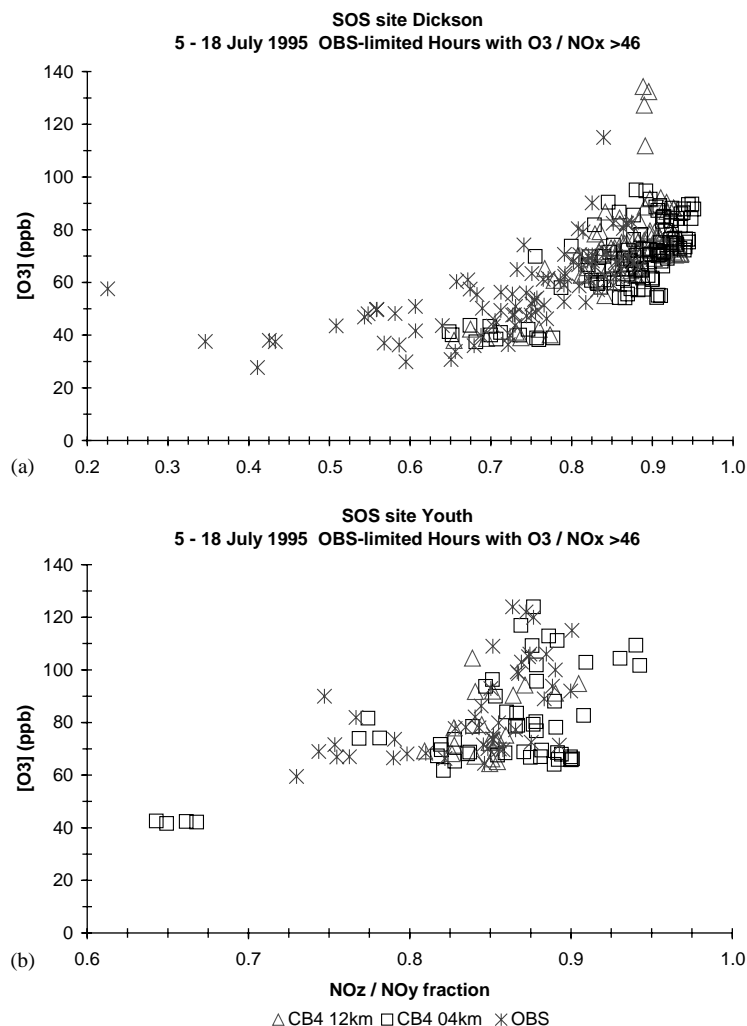


Fig. 8. (a), (b) [O₃] as a function of air mass age for the NO_x-limited conditions indicated by [O₃]/[NO_x] > 46, CB4 chemistry only, at (a) Dickson, and (b) Youth.

curve of [O₃] vs. [NO_Z] for the two very different sites, Dickson being rural and having lower maximum [O₃] and less NO_Z, and Youth being near-urban with higher [O₃] and relatively more NO_Z. CMAQ's intercept is slightly higher than that of the observations at Dickson, but we note that the models do reproduce the rather complicated curvature with decreasing NO_Z values. The line produced from all hours observed or simulated or even from hours in a specific time or chemical regime, has significant curvature at both ends as is evident in Fig. 9a. This curvature and the independence of both variables, O₃ and NO_Z, mean that traditional regression statistics will not correctly describe the relationship between the two. We describe that relationship qualitatively here, while continuing to search for and test new statistical techniques for quantification.

Points from the CMAQ grid model along the curve for Dickson can be displaced along the line of the curve most likely owing to the influence of the large-scale fresh NO_x plumes appearing in the grid models and altering the rates of P(O₃) and P(NO_Z). As before, preliminary results (not shown here) with the CMAQ embedded plume model PinG indicate improvement by containing the physical dispersal of the NO_x plume more realistically. At Youth, where more urban-like photochemistry predominates, CMAQ more correctly places the bulk of the distribution along the line of the observations. We interpret this to mean that the rates of photochemical processing in CMAQ are credible representations of those in the atmosphere. Two elements at work here. First, that P(O₃) and P(NO_Z) are controlled by the photochemical dynamics illustrated in Fig. 1, and

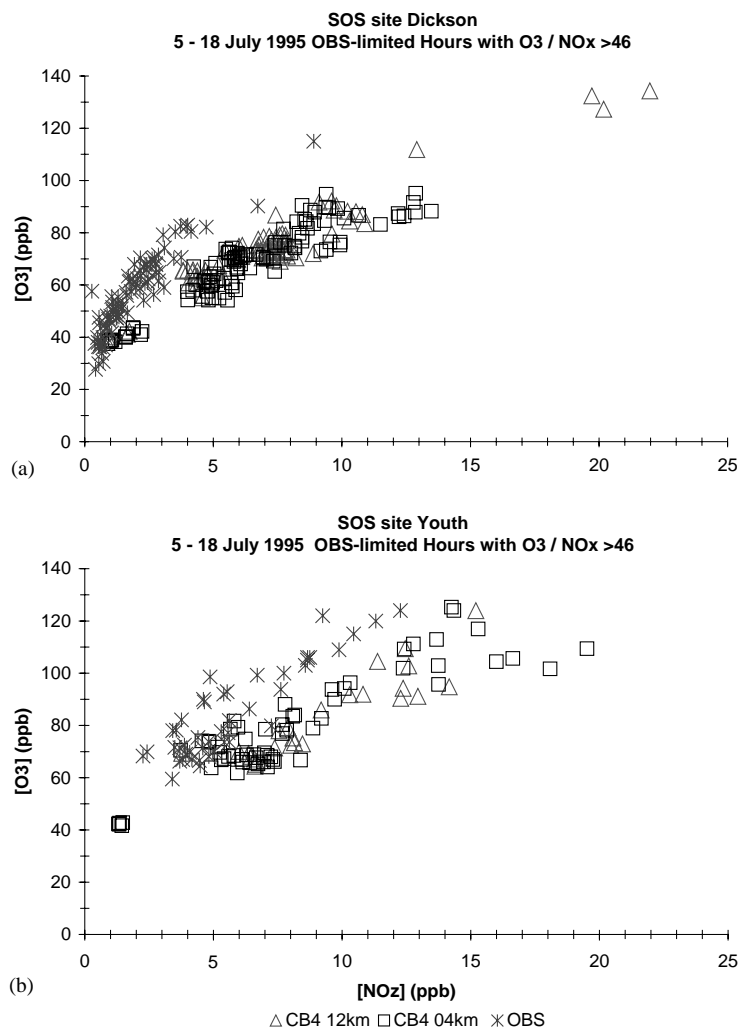


Fig. 9. (a), (b) [O₃] as a function of NO_Z in the NO_x-limited conditions indicated by [O₃]/[NO_x] > 46, CB4 chemistry only, at (a) Dickson, and (b) Youth.

second, that points in this comparison were filtered using the ridgeline indicator to select hours when the photochemical systems are strongly NO_x-limited. Thus, the slope of the model's curves being similar to that of the atmosphere means that O₃ and NO_Z are likely being produced in the model in a way similar to that of the atmosphere. If the photochemical processing is similar, then in cases where more NO_x is present in the grid model due to inappropriate treatment of large-scale physical plume dispersal as at Dickson, we expect that the model results would simply be displaced along the line of the curve, producing more O₃ and more NO_Z together, different from the observations in absolute totals, but having a similar slope over the days. We note that the slope of the line of the CB4 results appears flatter than that of the observations, but caution against interpreting this result too closely since a traditional

regression relationship will not correctly describe this curve.

5. Conclusions

The three diagnostic probes of photochemical dynamics discussed here provide robust and reliable process information chiefly about the aggregate production rate of O₃ and some details of NO_x cycling in determining that rate. Importantly, the three probes give consistent information about the model processes and are particularly useful when used together. For example, the [O₃] response surface indicator [O₃]/[NO_x] can broadly characterize a photochemical system: low values of the ratio tend to be associated with early morning periods when [NO_x] is high and [O₃] low, and higher

values of the ratio are associated with hours late in the photochemical day when conditions have reversed. However, the values of this ratio are not uniquely determined and could be ambiguous with regard to the response surface ridgeline if the system O_3 response were not also filtered by an indicator of air mass aging, the fraction NO_Z/NO_Y , for example. In a similar way, information about the production efficiency of O_3 per NO_X converted is sharpened significantly when filtered by the response surface indicator to be centered in the region of strongest NO_X limitation. Thus the power of the probes can be exploited more fully when applied together for building interpretations of atmospheric processes in the observations and in the model.

It is helpful to illustrate the utility and power of these probes with results from a model evaluation application. Application of the three diagnostic probes to CMAQ as discussed here has led us to these specific conclusions about the model's representation of photochemical dynamics.

For the most part, the model correctly reproduces differences in the transition of photochemical systems across their response surfaces at three SOS 95 surface sites as revealed by the $[O_3]$ response surface indicator $[O_3]/[NO_X]$; the model does well at the rural and near-urban site, but can still suffer when local source emissions are missing from model inputs as we believe to be the case for Giles; for understanding the placement of a system on the $[O_3]$ response surface, the 4 km models out-perform the 12 km ones; and for these tests, CMAQ results do not vary with the choice of chemical mechanism.

The model appears to be aging NO_X to NO_Z in an appropriate way as indicated by the observations at Dickson and Youth and is likely producing O_3 from NO_X cycling with processes and rates that are largely equivalent to those in the atmosphere, meaning that substantial deficiencies likely are not present in the model's chemical mechanisms.

Taken together, these tests applied in the NO_X -limited region of the $[O_3]$ response surface substantially increase our confidence that the model is performing correctly there.

We conclude that the insights derived from process-oriented probing of photochemical dynamics in the observations and in the model demonstrate the high utility of collecting the most accurate and chemically specific measurements of the key species in these processes, most especially NO_2 , for analysis and understanding of ambient photochemistry and its representation in numerical models.

Acknowledgements

Support for JRA is provided by the NOAA Atmospheric Sciences Modeling Division and administered by

the Visiting Scientist Program of the University Corporation for Atmospheric Research.

This paper has been reviewed in accordance with US EPA's peer review policies and approved for publication. Mention of trade names or commercial products does not constitute endorsement or recommendation for use.

References

- Arnold, J.R., Dennis, R.L., 2001. First results from operational testing of the US EPA Models-3/Community Multiscale Model for Air Quality (CMAQ). In: Gryning, S.-E., Schiermeier, F.A. (Eds.), *Air Pollution Modeling and Its Application XIV*. Kluwer Academic, Dordrecht, pp. 651–658.
- Arnold, J.R., Dennis, R.L., Tonnesen, G.S., 1998. Advanced techniques for evaluating Eulerian air quality models: background and methodology. In: *American Meteorological Society 10th Joint Conference on the Applications of Air Pollution Meteorology with the American Waste Management Association*, American Meteorological Society, Boston, pp. 1–5.
- Benjey, W.G., Godowitch, J.M., Gipson, G.L., 1999. Emission subsystem. In: Byun, D.W., Ching, J.K.S. (Eds.), *Science Algorithms of the EPA Models-3 Community Multi-scale Air Quality (CMAQ) Modeling System*. US EPA Report No. EPA/600/R-99/030, Office of Research and Development, Washington, DC (Chapter 4).
- Byun, D.W., Ching, J.K.S. (Eds.), 1999. *Science Algorithms of the EPA Models-3 Community Multi-scale Air Quality (CMAQ) Modeling System*. US EPA Report No. EPA/600/R-99/030, Office of Research and Development, Washington, DC.
- Carter, W.P.L., 1996. Condensed atmospheric photooxidation mechanisms for isoprene. *Atmospheric Environment* 24, 4275–4290.
- Dennis, R.L., Arnold, J.R., Tonnesen, G.S., 2000. On the need for better ambient observations of important chemical species for air quality model evaluation. In: McClenny, W.A. (Ed.), *Recommended Methods for Ambient Air Monitoring of NO, NO₂, NO_y, and Individual NO_Z Species*, EPA Report No. EPA-600/R-01/005, Office of Research and Development, Research Triangle Park (Chapter 4).
- Dennis, R.L., Arnold, J.R., Tonnesen, G.S., 2002. Probing the shores of ignorance. In: Beck, M.B. (Ed.), *Environmental Foresight and Models: A Manifesto*. Elsevier, New York, (Chapter 17).
- Dodge, M.C., 1977. Combined use of modeling techniques and smog chamber data to derive ozone precursor relationships. In: Dimitriadis, B. (Ed.), *Proceedings of the International Conference on Photochemical Oxidant Pollution and Its Control*, US EPA Report No. EPA-600/3-77-001b, Office of Research and Development, Research Triangle Park.
- Gery, M.W., Whitten, G.Z., Killus, J.P., Dodge, M.C., 1989. A photochemical kinetics mechanism for urban and regional scale computer modeling. *Journal of Geophysical Research* 94, 12925–12956.

- Gillani, N.V., Godowitch, J.M., 1999. Plume-in-grid treatment of major point source emissions. In: Byun, D.W., Ching, J.K.S. (Eds.), Science Algorithms of the EPA Models-3 Community Multi-scale Air Quality (CMAQ) Modeling System, US EPA Report No. EPA/600/R-99/030, Office of Research and Development, Washington, DC (Chapter 9).
- Gipson, G.L., 1999. Process analysis. In: Byun, D.W., Ching, J.K.S. (Eds.), Science Algorithms of the EPA Models-3 Community Multi-scale Air Quality (CMAQ) Modeling System, US EPA Report No. EPA/600/R-99/030, Office of Research and Development, Washington, DC (Chapter 8).
- Grell, G.A., Dudhia, J., Stauffer, D.R., 1994. A description of the fifth-generation Penn State. NCAR mesoscale model (MM5), NCAR Technical Note, NCAR/TN-398+STR, Boulder.
- Jacobson, M.Z., Turco, R.P., 1994. SMVGEAR: a sparse-matrix, vectorized gear code for atmospheric models. *Atmospheric Environment A* 28, 273–284.
- Kleinman, L.I., 1994. Low- and high-NO_x tropospheric photochemistry. *Journal of Geophysical Research* 99, 16831–16838.
- Kleinman, L., Daum, P., Lee, Y., Springston, S., Newman, L., Leaitch, W., Banic, C., Issac, G., MacPherson, J., 1996a. Measurement of ozone and related compounds over southern Nova Scotia 1. Vertical distributions. *Journal of Geophysical Research* 101, 29043–29060.
- Kleinman, L., Daum, P., Springston, S., Leaitch, W., Banic, C., Issac, G., Jobson, B., Niki, H., 1996b. Measurement of ozone and related compounds over southern Nova Scotia 2. Photochemical age and vertical transport. *Journal of Geophysical Research* 101, 29061–29074.
- Meagher, J.F., Cowling, E.B., Fehsenfeld, F.C., Parkhurst, W.J., 1998. Ozone formation and transport in the southeastern United States: overview of the SOS Nashville/Middle Tennessee ozone study. *Journal of Geophysical Research* 103, 22213–22223.
- Milford, J., Gao, D., Sillman, S., Blosser, P., Russell, A., 1994. Total reactive nitrogen (NO_y) as an indicator for the sensitivity of ozone to NO_x and hydrocarbons. *Journal of Geophysical Research* 99, 3533–3542.
- National Research Council, 1991. Rethinking the Ozone Problem in Urban and Regional Air Pollution. National Academy Press, Washington, DC.
- Olszyna, K.J., 2002. Personal communication to RLD.
- Olszyna, K.J., Parkhurst, W.J., Meagher, J.F., 1998. Air chemistry during the 1995 SOS/Nashville intensive determined from level 2 network. *Journal of Geophysical Research* 103, 31143–31153.
- Parish, D., Buhr, M., Trainer, M., Norton, R., Shimshock, J., Fehsenfeld, F., Anlauf, G., Bottenheim, J., Tang, Y., Wiebe, H., Roberts, J., Tanner, R., Newman, L., Bowersox, V., Olszyna, K., Bailey, E., Rodgers, M., Wang, T., Berresheim, H., Roychowdhury, U., Demerjian, K., 1993. The total reactive oxidized nitrogen levels and the partitioning between the individual species at six rural sites in eastern North America. *Journal of Geophysical Research* 98, 2927–2939.
- Russell, A., Dennis, R., 2000. NARSTO critical review of photochemical models and modeling. *Atmospheric Environment* 34, 2283–2324.
- Seinfeld, J.H., Pandis, S., 1998. *Atmospheric Chemistry and Physics: From Air Pollution to Climate Change*. Wiley, New York.
- Senff, C.J., Hardesty, R.M., Alvarez II, R.J., Mayor, S.D., 1998. Airborne lidar characterization of power plant plumes during the 1995 Southern oxidants study. *Journal of Geophysical Research* 105, 31173–31189.
- Sillman, S., 1995. The use of NO_y, H₂O₂, and HNO₃ as indicators for ozone-NO_x-hydrocarbon sensitivity in urban locations. *Journal of Geophysical Research* 100, 14175–14188.
- Sillman, S., He, D., Cardelino, C., Imhoff, R., 1997. The use of photochemical indicators to evaluate ozone-NO_x-hydrocarbon sensitivities: case studies from Atlanta, New York, and Los Angeles. *Journal of the Air and Waste Management Association* 47, 642–652.
- Stockwell, W.R., Middleton, P., Chang, J.S., Tang, X., 1990. The second generation regional acid deposition model chemical mechanism for regional air quality modeling. *Journal of Geophysical Research* 95, 16343–16357.
- Tonnesen, G.S., Dennis, R.L., 2000a. Analysis of radical propagation efficiency to assess ozone sensitivity to hydrocarbons and NO_x. Part I: local indicators of instantaneous odd oxygen production sensitivity. *Journal of Geophysical Research* 105, 9213–9225.
- Tonnesen, G.S., Dennis, R.L., 2000b. Analysis of radical propagation efficiency to assess ozone sensitivity to hydrocarbons and NO_x. Part II: long-lived species as indicators or ozone concentration sensitivity. *Journal of Geophysical Research* 105, 9227–9241.
- Trainer, M., Parish, D., Buhr, M., Norton, R., Fehsenfeld, F., Anlauf, G., Bottenheim, J., Tang, Y., Wiebe, H., Roberts, J., Tanner, R., Newman, L., Bowersox, V., Meagher, J., Olszyna, K., Rodgers, M., Wang, T., Berresheim, H., Demerjian, K., Roychowdhury, U., 1993. Correlation of ozone with NO_y in photochemically aged air. *Journal of Geophysical Research* 98, 2917–2925.
- US Environmental Protection Agency (US EPA), 1997. Regulatory Impact Analyses for the Particulate Matter and Ozone National Ambient Air Quality Standards and Proposed Regional Haze Rule. US EPA Office of Air Quality Planning and Standards, Research Triangle Park.
- Valente, R., Imhoff, R., Tanner, R., Meagher, J., Daum, P., Hardesty, R., Banta, R., Alvarez, R., McNider, R., Gillani, N., 1998. Ozone production during an urban air stagnation episode over Nashville, Tennessee. *Journal of Geophysical Research* 103, 2255–2256.